Science Advances
AAAS

Supplementary Materials for

Cytokine-scavenging nanodecoys reconstruct osteoclast/osteoblast balance toward the treatment of postmenopausal osteoporosis

Yang Zhou, Yekun Deng, Zhongmin Liu, Mengyuan Yin, Mengying Hou, Ziyin Zhao, Xiaozhong Zhou, Lichen Yin*

*Corresponding author. Email: lcyin@suda.edu.cn

Published 24 November 2021, *Sci. Adv.* **7**, eabl6432 (2021)
DOI: 10.1126/sciadv.abl6432

This PDF file includes:

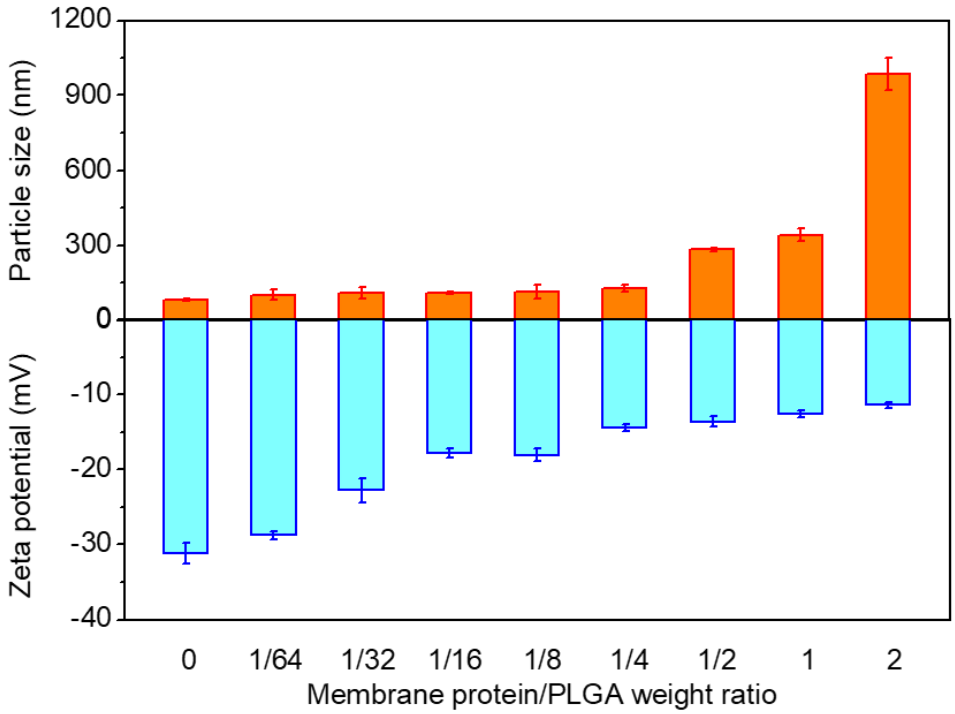

Fig. S1.

Particle size and zeta potential of RAW-PLGA nanodecoys at different membrane protein/PLGA weight ratios in water.

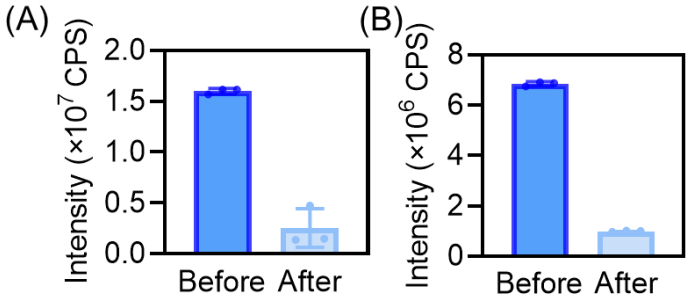

Fig. S2.

Membrane coating efficiency of RAW-PLGA nanodecoys. (**A**) Fluorescence intensity of RAW-^{DiD}PLGA nanodecoys (1 mg ^{DiD}PLGA/mL) before and after centrifugation (10,000 g, 10 min) (*n* = 3). (**B**) Fluorescence intensity of ^{DiD}RAW-PLGA nanodecoys (1 mg PLGA/mL) before and after centrifugation (10,000 g, 10 min) (*n* = 3).

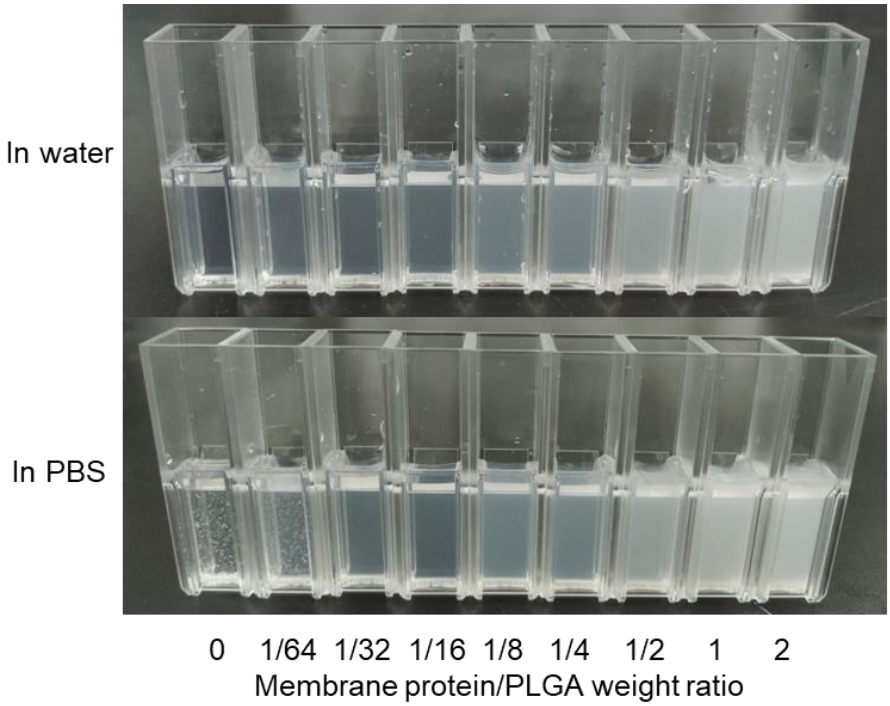

Fig. S3.

Images of RAW-PLGA nanodecoys in water or PBS at different membrane protein/PLGA weight ratios. Photo Credit: Yang Zhou, Institute of Functional Nano & Soft Materials (FUNSOM), Jiangsu Key Laboratory for Carbon-Based Functional Materials and Devices, Soochow University.

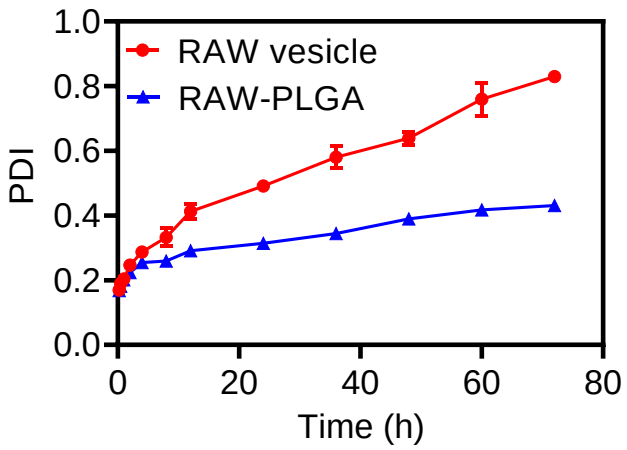

Fig. S4.

Alteration of the PDI of RAW vesicles and RAW-PLGA nanodecoys after incubation in DMEM containing 10% FBS for different time (n = 3).

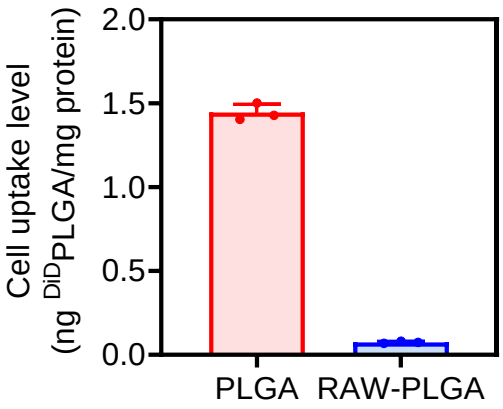

Fig. S5.

Uptake levels of ^{DiD}PLGA NPs and RAW-^{DiD}PLGA nanodecoys (100 μg ^{DiD}PLGA/mL) in RAW 264.7 cells following incubation for 4 h (n = 3).

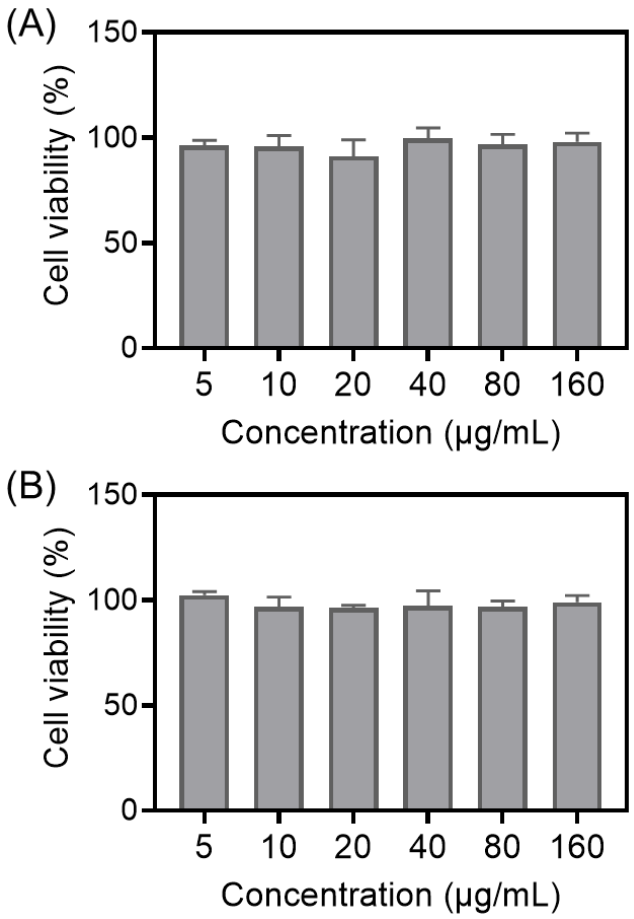

Fig. S6.

Viability of RAW 264.7 cells (**A**) and MC3T3-E1 cells (**B**) following 24-h incubation with RAW-PLGA nanodecoys at various PLGA concentrations (n = 3).

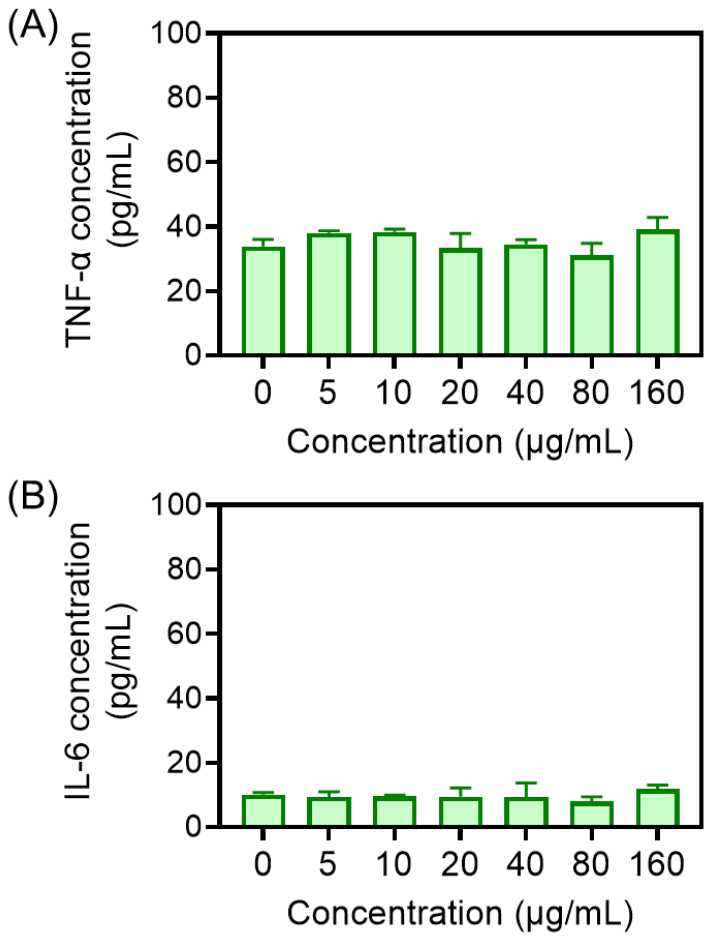

Fig. S7.

Immunostimulatory properties of RAW-PLGA nanodecoys. TNF-α (**A**) and IL-6 (**B**) secretion levels of RAW 264.7 cells following 24-h incubation with RAW-PLGA nanodecoys at various PLGA concentrations (n = 3).

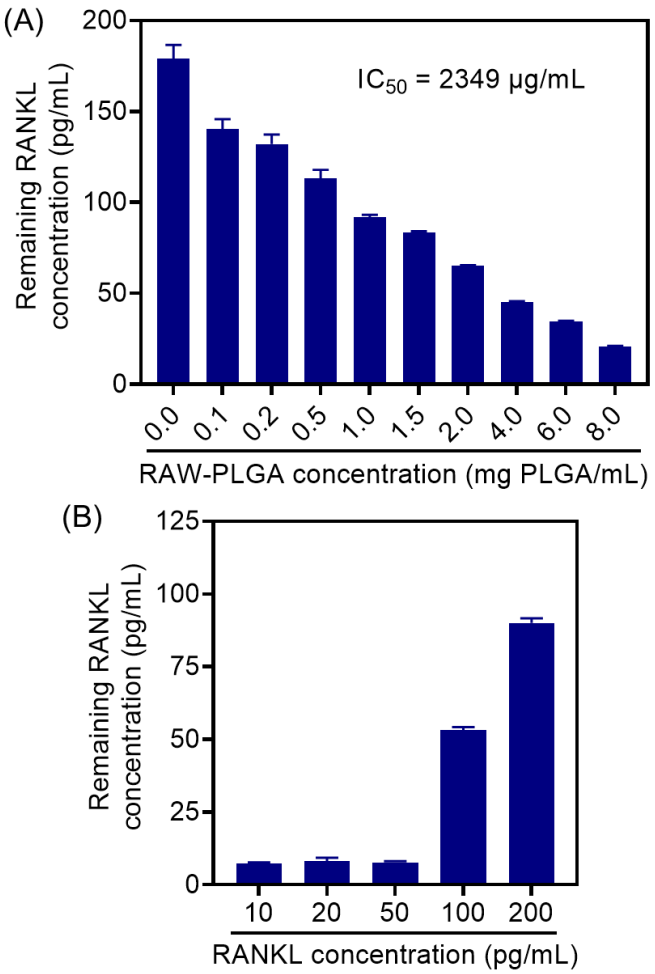

Fig. S8.

Dose-dependent scavenging of RANKL by RAW-PLGA nanodecoys. (**A**) RANKL scavenging efficiencies of RAW-PLGA nanodecoys at various concentrations when the RANKL concentration was maintained at 200 pg/mL (n = 3). (**B**) RANKL scavenging efficiencies of RAW-PLGA nanodecoys (1 mg PLGA/mL) when the RANKL concentrations were varied from 10 to 200 pg/mL (n = 3).

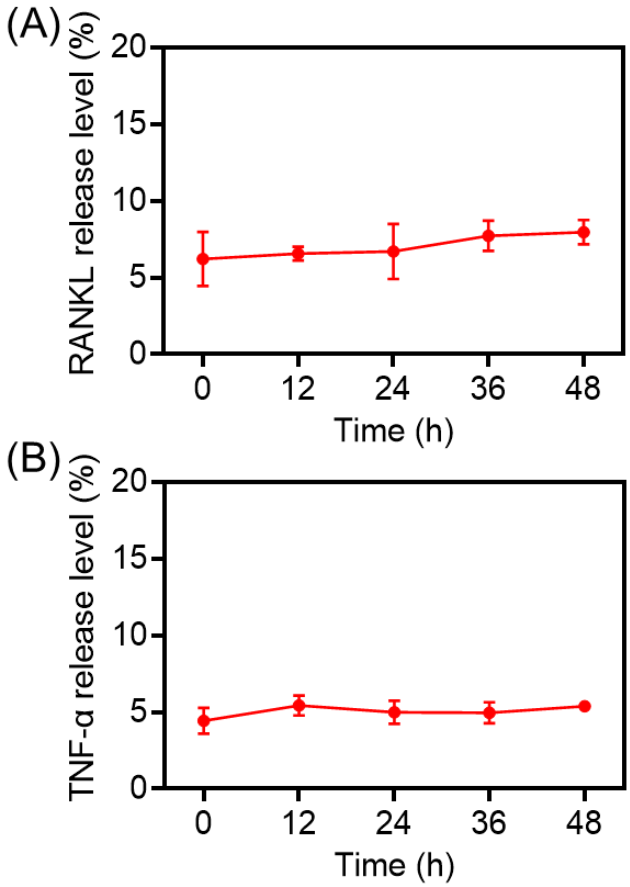

Fig. S9.

Cytokine release from the cytokine/RAW-PLGA complexes. Cumulative RANKL (**A**) or TNF-α (**B**) release from RAW-PLGA nanodecoys that had bound RANKL or TNF-α after incubation in DMEM containing 10% FBS for different time (n = 3).

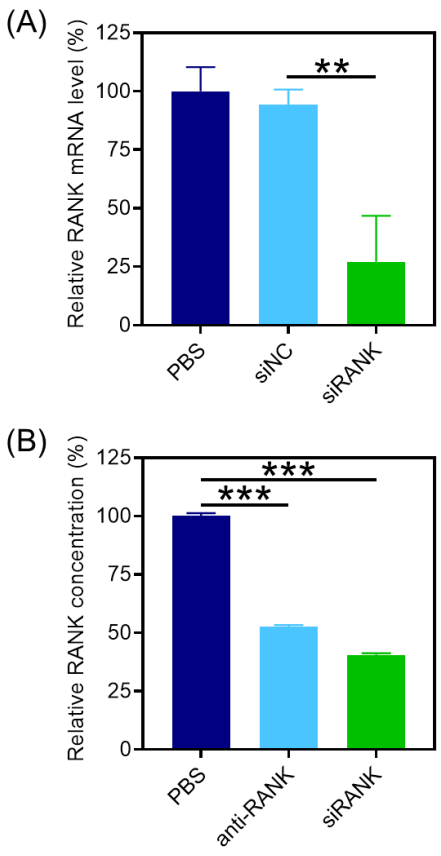

Fig. S10.

Down-regulation of the RANK level in RAW 264.7 cells after siRANK or anti-RANK treatment. (**A**) Relative RANK mRNA level in RAW 264.7 cells after incubation with different nanocomplexes (LPF2000/siNC and LPF2000/siRANK, w/w = 1:1) as determined by real-time PCR (n = 3). (**B**) Relative RANK protein level in RAW 264.7 cells after incubation with PBS, anti-RANK, or LPF2000/siRANK nanocomplexes as determined by ELISA (n = 3).

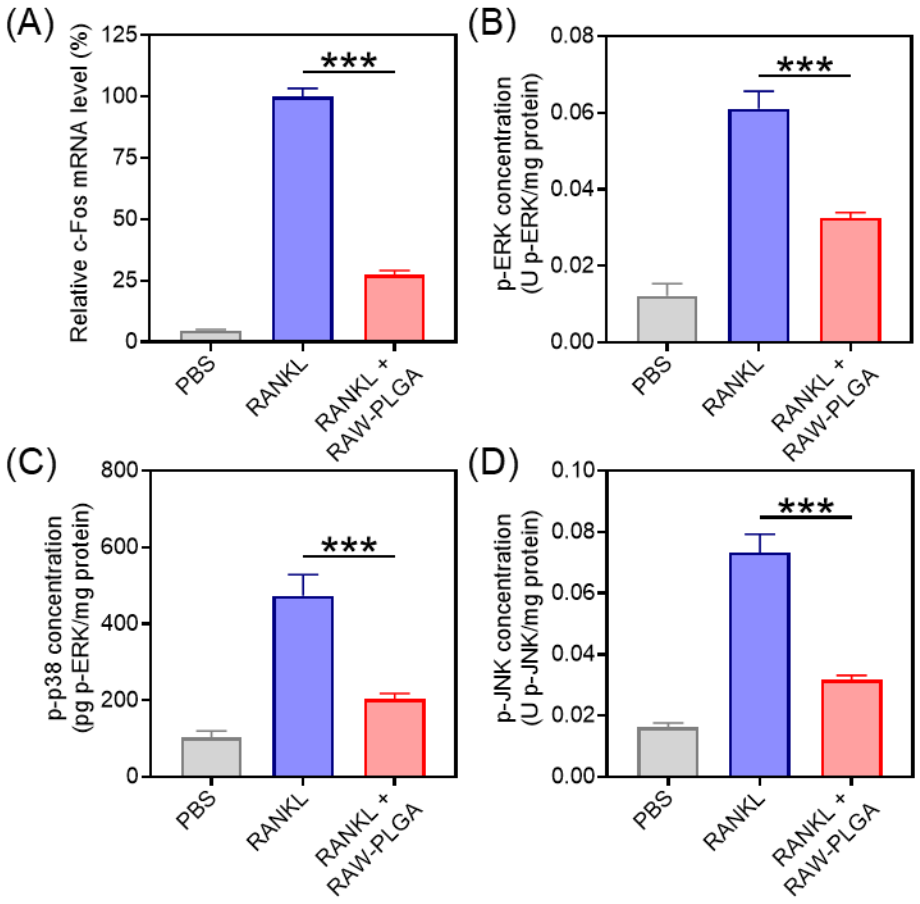

Fig. S11.

RAW-PLGA nanodecoys-mediated blocking of the NF-κB and MAPK pathways. Relative c-Fos mRNA level (**A**) and p-ERK (**B**), p-p38 (**C**), and p-JNK (**D**) levels in RAW 264.7 cells (n = 3).

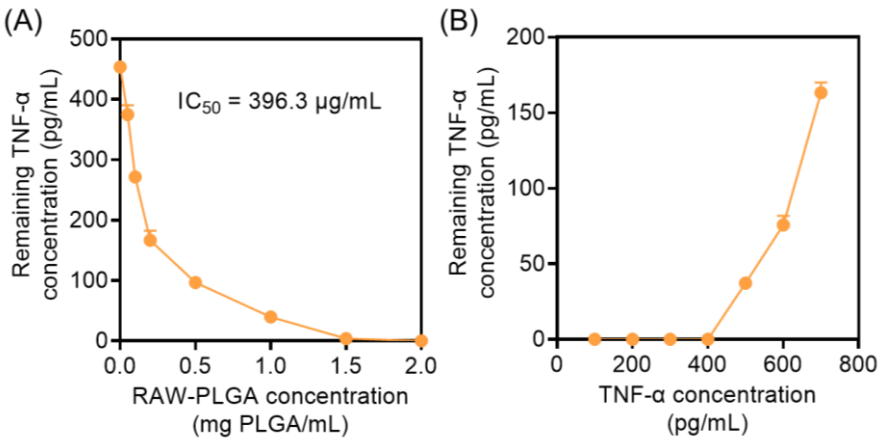

Fig. S12.

Dose-dependent scavenging of TNF-α by RAW-PLGA nanodecoys. (**A**) TNF-α scavenging efficiencies of RAW-PLGA nanodecoys at various concentrations when the TNF-α concentration was maintained at 500 pg/mL (n = 3). (**B**) TNF-α scavenging efficiencies of RAW-PLGA nanodecoys (1 mg PLGA/mL) when the TNF-α concentrations were varied from 100 to 700 pg/mL (n = 3).

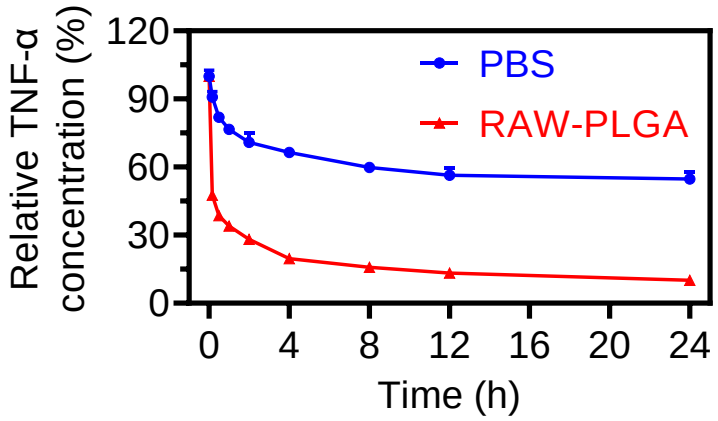

Fig. S13.

Extracellular TNF-α concentration of MC3T3-E1 cells after incubation with PBS or RAW-PLGA nanodecoys for different time at the initial TNF-α concentration of 100 ng/mL (n = 3).

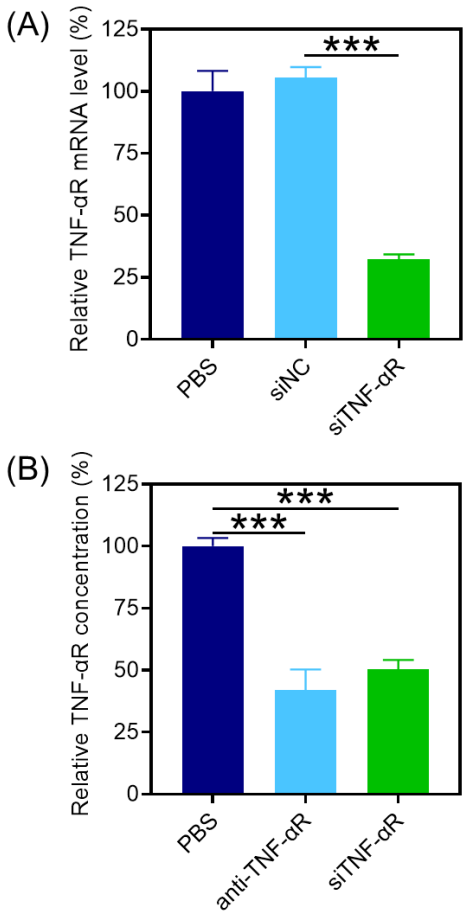

Fig. S14.

Down-regulation of the TNF-αR level in RAW 264.7 cells after siTNF-αR or anti-TNF-αR treatment. (**A**) Relative TNF-αR mRNA level in RAW 264.7 cells after incubation with different nanocomplexes (LPF2000/siNC and LPF2000/siTNF-αR, w/w = 1:1) as determined by real-time PCR (n = 3). (**B**) Relative TNF-αR protein level in RAW 264.7 cells following treatment with LPPF2000/siTNF-αR nanocomplexes or anti-TNF-αR (n = 3).

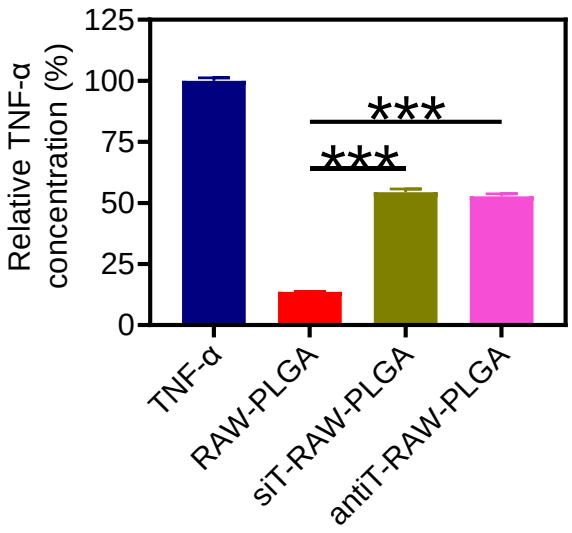

Fig. S15.

TNF-α scavenging efficiencies of RAW-PLGA nanodecoys, antiT-RAW-PLGA nanodecoys, and siT-RAW-PLGA nanodecoys at the initial TNF-α concentration of 500 pg/mL (n = 3).

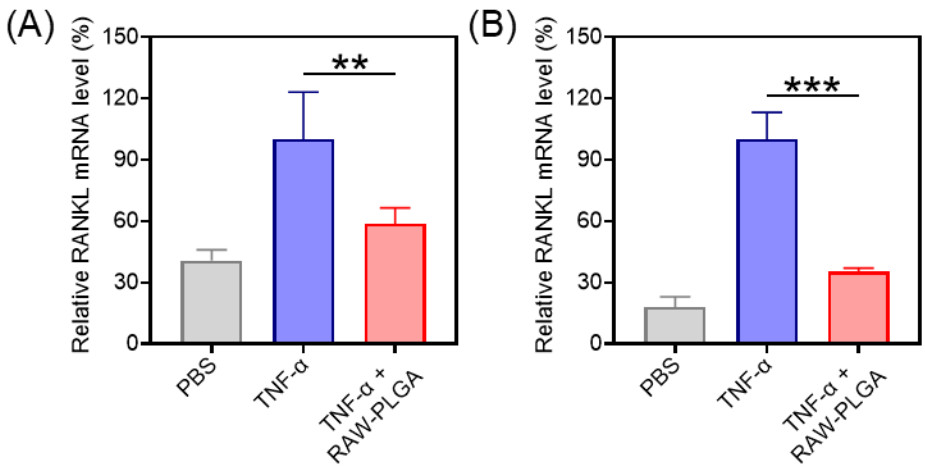

Fig. S16.

RAW-PLGA nanodecoys-mediated RANKL down-regulation after TNF-α challenge. Relative RANKL mRNA level in TNF-α-challenged RAW 264.7 cells (**A**) and MC3T3-E1 cells (**B**) following incubation with RAW-PLGA nanodecoys (n = 3).

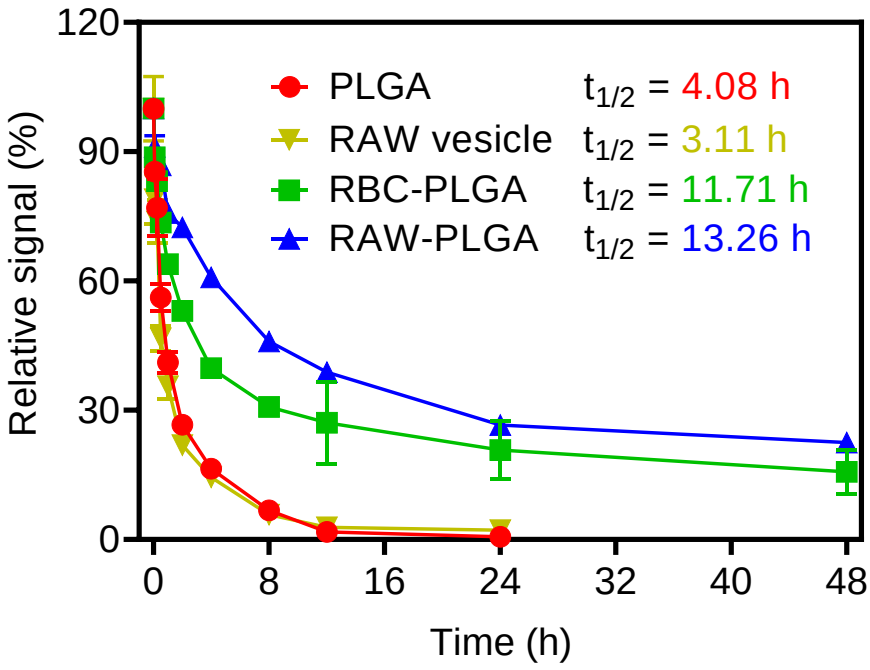

Fig. S17.

Pharmacokinetics of ^{DiD}PLGA NPs, ^{DiD}RAW vesicles, RBC-^{DiD}PLGA NPs, or RAW-^{DiD}PLGA nanodecoys in mice following *i.v.* injection at 10 mg ^{DiD}PLGA/kg or 2.5 mg ^{DiD}RAW vesicles/kg (n = 3).

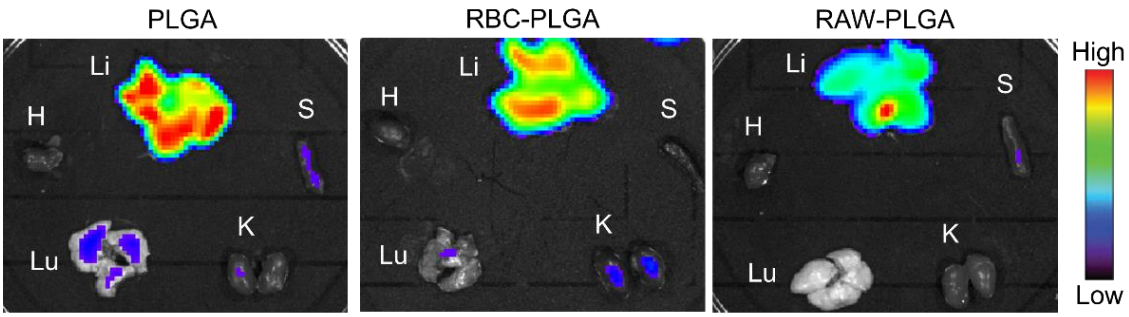

Fig. S18.

Ex vivo fluorescence imaging of excised major organs at 24 h post *i.v.* injection of ^{DiD}PLGA NPs, RBC-^{DiD}PLGA NPs, or RAW-^{DiD}PLGA nanodecoys at 10 mg ^{DiD}PLGA/kg (H: heart; Lu: lung; S: spleen; K: kidney; Li: liver).

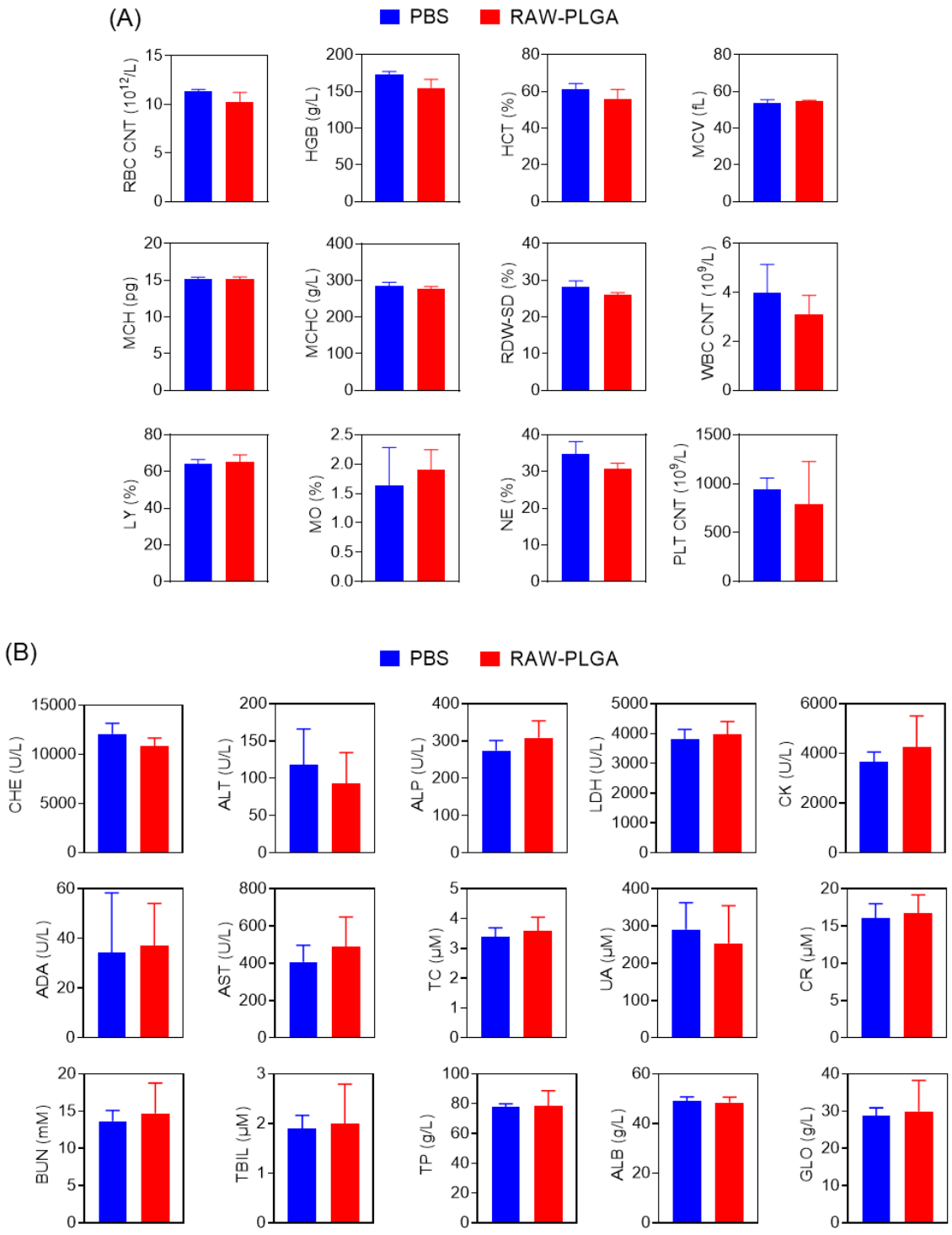

Fig. S19.

Biocompatibility of RAW-PLGA nanodecoys. Hematological (**A**) and biochemical (**B**) parameters of mice after *i.v.* injection of PBS and RAW-PLGA nanodecoys (10 mg/kg) (n = 3).

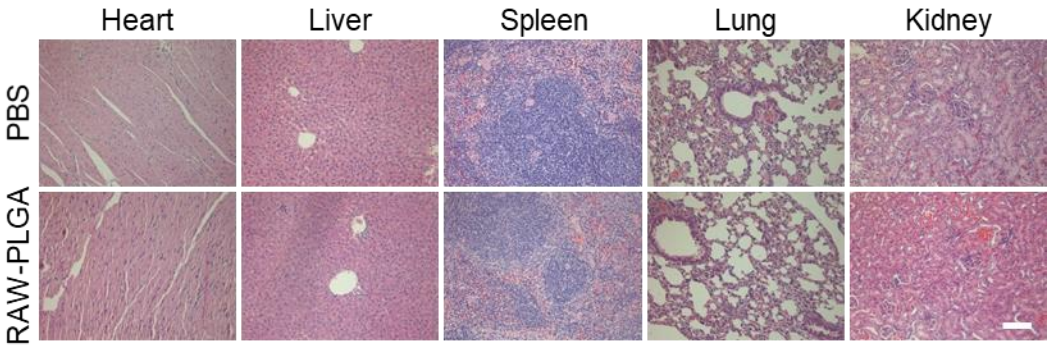

Fig. S20.

H&E-stained major organ sections of mice after *i.v.* injection of PBS or RAW-PLGA nanodecoys (10 mg PLGA/kg) (scale bar = 100 μm).

Table S1.

Sequences of primers used for the real-time PCR analysis.

Primers	Forward	Reverse
RANK	5′-AGATGTGGTCTGCAGCTCTTCCAT-3′	5′-ACACACTTCTTGCTGACTGGAGGT-3′
TNF-αR	5′-GGAAAGTATGTCCATTCTAAGAACAA-3′	5′-GTCACTCACCAAGTAGGTTCCTT-3′
c-Fos	5′-TTTCAACGCGGACTACGAGG-3′	5′-GCGCAAAAGTCCTGTGTGTT-3′
RANKL	5′-CAGAAGGAACTGCAACACAT-3′	5′-CAGAGTGACTTTATGGGAACC-3′
TNF-α	5′-TGATCCGAGATGTGGAACTG-3′	5′-CGAGCAGGAATGAGAAGAGG-3′
IL-6	5′-CAATCTGGGTTCAATCAGGCGAT-3′	5′-GCATCTTCTCCAGCAGGTCAG-3′
IL-1β	5′-CCCAAGCAATACCCAAAGAA-3′	5′-GCTTGTGCTCTGCTTGTGAG-3′
RUNX2	5′-GGCAGTTCCCAAGCATTTCA-3′	5′-GGTAAAGGTGGCTGGGTAGT-3′
OSX	5′-CCTCTCGACCCGACTGCAGATC-3′	5′-AGCTGCAAGCTCTCTGTAACCATGAC-3′
OSC	5′-AAGCAGGAGGGCAATAAGGT-3′	5′-CAAGCAGGGTTAAGCTCACA-3′
TRAF6	5′-TTGCACATTCAGTGTTTTTGG-3′	5′-TGCAAGTGTCGTGCCAAG-3′
NFATc1	5′-CCGTTGCTTCCAGAAAATAACA-3′	5′-TGTGGGATGTGAACTCGGAA-3′
ctsK	5′-AGCGAACAGATTCTCAACAGC-3′	5′-AGACAGAGCAAAGCTCACCAT-3′
TRAP	5′-CGTCTCTGCACAGATTGCAT-3′	5′-AAGCGCAAACGGTAGTAAGG-3′
RECK	5′--CTCCAGCAGTCTCCCGTCAT-3′	5′-GTTGTGGGTGGTCAGGGTCTA-3′
MMP-2	5′-GCAATACCTGAACACTTTCTATG-3′	5′-TCTGGTCAAGGTCACCTGTC-3′
MMP-9	5′-TGGCAGAGGCATACTTGTACC-3′	5′-TGTCCAGCTCACCAGTCT-3′
MMP-13	5′-CTGGACCAAACTATGGTGGG-3′	5′-GGTCCTTGGAGTGATCCAGA-3′
GAPDH	5’-TTCACCACCATGGAGAAGGC-3’	5’-GGCATGGACTGTGGTCATGA-3

Table S2.
Abbreviations of various hematological parameters.

Full name	Abbreviation
Red blood cell count	RBC CNT
Hemoglobin	HGB
Hematocrit	HCT
Mean corpuscular volume	MCV
Mean corpuscular hemoglobin	MCH
Mean corpuscular hemoglobin concentration	MCHC
Standard deviation of red blood cell distribution width	RDW-SD
White blood cell count	WBC CNT
% lymphocyte	LY
% monocyte	MO
% neutrophil	NE
Platelet count	PLT CNT

Table S3.

Abbreviations of various biochemical parameters.

Full name	Abbreviation
Cholinesterase	CHE
Alanine aminotransferase	ALT
Alkaline phosphatase	ALP
Lactate dehydrogenase	LDH
Creatine kinase	CK
Adenosine deaminase	ADA
Aspartate amino transferase	AST
Total cholesterol	TC
Uric acid	UA
Creatinine	CR
Blood urea nitrogen	BUN
Total bilirubin	TBIL
Total protein	TP
Albumin	ALB
Globulin	GLO